ORIGINAL RESEARCH



WILEY

Image processing setting adaptions according to image dose and radiologist preference can improve image quality in computed radiography of the equine distal limb: A cadaveric study

Clinical Unit of Diagnostic Imaging, Department for Companion Animals and Horses, University of Veterinary Medicine, Vienna, Austria

Correspondence

Matthias Seeber, Clinical Unit of Diagnostic Imaging, Department for Companion Animals and Horses, University of Veterinary Medicine, 1210 Vienna, Austria.

Email: Matthias.Seeber@vetmeduni.ac.at

Abstract

Image processing (IP) in digital radiography has been steadily refined to improve image quality. Adaptable settings enable users to adjust systems to their specific requirements. This prospective, analytical study aimed to investigate the influence of different IP settings and dose reductions on image quality. Included were 20 cadaveric equine limb specimens distal to the metacarpophalangeal and metatarsophalangeal joints. Images were processed with the Dynamic Visualization II system (Fujifilm) using five different IP settings including multiobjective frequency processing, flexible noise control (FNC), and virtual grid processing (VGP). Seven criteria were assessed by three veterinary radiology Diplomates and one veterinary radiology resident in a blinded study using a scoring system. Algorithm comparison was performed using an absolute visual grading analysis. The rating of bone structures was improved by VGP at full dose (P < .05; AUC $_{VGC}$ = 0.45). Überschwinger artifact perception was enhanced by VGP (P < .001; AUC $_{VGC}$ = 0.66), whereas image noise perception was suppressed by FNC (P < .001; AUC_{VGC} = 0.29). The ratings of bone structures were improved by FNC at 50% dose (P < .05; AUC $_{VGC}$ = 0.44), and 25% dose (P < .001; AUC $_{VGC}$ = 0.32), and clinically acceptable image quality was maintained at 50% dose (mean rating 2.16; 95.8% ratings sufficient or better). The favored IP setting varied among observers, with higher agreement at lower dose levels. These findings supported using individualized IP settings based on the radiologist's preferences and situational image requirements, rather than using default settings.

KEYWORDS

exposure dose, image quality, multiscale processing, post-processing, scatter correction

This is an open access article under the terms of the Creative Commons Attribution-NonCommercial-NoDerivs License, which permits use and distribution in any medium, provided the original work is properly cited, the use is non-commercial and no modifications or adaptations are made.

© 2023 The Authors. Veterinary Radiology & Ultrasound published by Wiley Periodicals LLC on behalf of American College of Veterinary Radiology.



1 | INTRODUCTION

Image quality (IQ) is critical for optimal diagnostic accuracy in equine orthopedic radiography. Poor-quality radiographs are difficult to evaluate, and they might be misinterpreted. 1 IQ in a digital radiography system is determined by the interaction of individual steps of the imaging chain: signal detection, signal processing, image display, data transmission, and data archiving.² Image processing (IP) is the procedure of converting the recorded detector signal into an image appropriate for clinical use³: the technical principle is to decompose the image into a series of subfrequency images and then to fuse these into one single image with improved structure visibility.^{4,5} IP software is continuously improved by manufacturers of digital radiography systems (e.g., Fujifilm's software Dynamic Visualization II). Recent expansions include four major tools: (1) gradation processing (GP) to optimize image contrast and density, 6 (2) multiobjective frequency processing (MFP) including frequency enhancement (FE) to enhance acutance in high spatial frequencies and dynamic range control (DRC) to increase visibility range,⁵ (3) flexible noise control (FNC) to reduce undesired image noise, 4 and (4) virtual grid processing (VGP) to virtually minimize the impact of scatter radiation. Very few studies specifically address veterinary applications of IP^{8-11} and focus on the equine distal limb.¹²

Both image noise and scatter radiation can lead to loss of diagnostic details. 13 Compared with conventional film/screen combinations, digital radiography has a wide dynamic range. However, underexposure results in grainy images, as image noise is inversely correlated with the amount of radiation the detector receives. 14 Noise reduction software can improve IQ in low-dose orthopedic radiography. 15 Scatter radiation, on the other hand, is related to the object size and compromises IQ by decreasing the signal-to-noise ratio and image contrast. 13 Scatter correction software can replace the physical grid without IQ impairment in orthopedic radiography¹⁶ and improve IQ in large-animal thoracic radiography. 10 However, the potential of FNC for dose reduction and VGP for IQ improvement has not yet been investigated in equine orthopedics. Conversely, insufficient processing can lead to the suppression of relevant image information and induction of artifacts. 1,17 For example, excessive IP may cause Überschwinger artifacts—a radiolucent halo occurring where large density differences exist between adjacent objects that can be mistaken for loosening of orthopedic devices¹ or pneumothorax.¹⁷ Modern software, like Dynamic Visualization II, 18 claims to be able to minimize this effect. ¹⁷ In our experience, inappropriate IP settings can still lead to disturbing artifacts; however, this has not yet been investigated in equine orthopedic radiography. Most software allows users to manually adapt IP settings to suit their individual needs and design their own protocols. Previous studies have demonstrated the potential of IP setting adaptation to improve the visibility of specific hard-to-detect structures, such as foreign bodies. 11 In phantom 19 and clinical 7,8 studies, modified processing resulted in a substantially reduced detector dose while maintaining the IQ level. In our experience, veterinary digital radiography systems often use IP protocols that were originally designed for human medical applications. It can be assumed that these protocols are not optimal given the considerable differences in subject sizes and variable structural features. However, the potential of IP setting adaptation has not yet been investigated in equine orthopedic radiography.

The aims of the study were to (1) investigate the effects of different IP settings on the IQ of radiographs of distal equine limbs; (2) assess the effects of low detector doses on IQ; (3) clarify whether by applying alternative processing algorithms, an acceptable IQ can still be achieved at low dose levels; (4) investigate the influence of the observer on the ratings of image features. Our hypotheses were as follows: (1) different IP settings have an influence on the perception of predefined image criteria of the distal equine limb; (2) VGP can improve the perception of anatomic structures; (3) FNC can improve the perception of anatomic structures at low levels of detector doses; (4) the effects of IP settings differ between full and low levels of detector doses, and an acceptable IQ can be achieved at low doses by applying alternative IP settings; (5) the preference regarding IP algorithms differs among observers.

2 | METHODS

2.1 | Selection and description of subjects

This study had a prospective analytical design. Ten forelimbs and 10 hindlimbs distal to the metacarpophalangeal and metatarsophalangeal joints of 20 horse cadavers were included. The sample size was based on previous visual grading studies with a comparable prospective analytical study design for radiographic IQ comparisons. \$16,20-23\$ The animals were euthanized for reasons unrelated to the study and had no evidence of orthopedic disease. The director of our department approved the use of cadavers for the analytical study, and patient data were not included. This study was not classified as an animal experiment by the local Animal Welfare Committee (Ethics Committee of the University for Veterinary Medicine, Vienna); therefore, the requirement for ethics approval was waived.

Inclusion criteria were as follows: (1) a hoof diameter (heel to dorsal coronary band distance) of $11.5\pm1.0~{\rm cm}$ to reduce interphantom variability and to perform the study with a standardized dose level and (2) no radiologically detectable abnormalities in the regions of interest. All decisions regarding subject inclusion or exclusion were consensually made by an ECVDI-certified veterinary radiologist (E.L.) and a graduate student (M.S.). The horseshoe was removed (if present), as well as any metal (if possible), to prevent any potential influence on preprocessing 17 and dose indicator 14 values. The limbs were cleaned and trimmed. Packing of the frog grooves was not performed.

For IP, the Dynamic Visualization II software (Fujifilm) on the work-station FCR Profect CP Plus (Fujifilm) was used, offering multiple adaptable processing tools (visualized and explained in Supporting Information S1). Because setting recommendations for equine distal limbs do not exist, different IP algorithms were defined in the first stage of the study. The IP algorithms were defined by a graduate student with experience in radiology (M.S.) under the supervision of an ECVDI board-certified veterinary radiologist (E.L.). To generate a

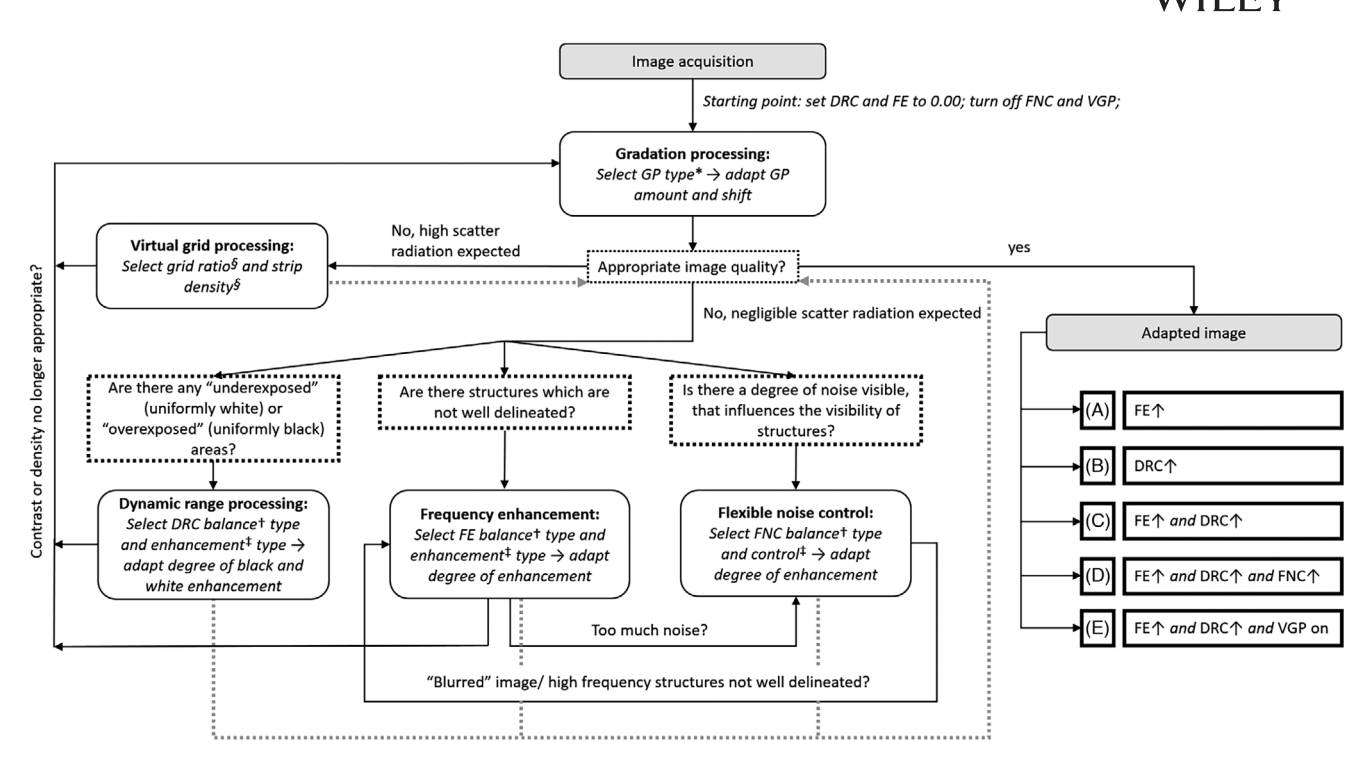


FIGURE 1 Flowchart showing the stepwise adjustment of IP parameters. A–E, five individually adapted algorithms. *According to the investigated region; †According to the object size; ‡According to the object density; \$According to the expected amount of scatter radiation. DRC, dynamic range control; FE, frequency enhancement; FNC, flexible noise control; GP, gradation processing; IP, image processing; VGP, virtual grid processing.

basic optimized IP setting, a systematic stepwise adjustment method developed in a previous study for comparable software²⁴ was adapted for the Dynamic Visualization II system (Figure 1). Images at 100% dose not included in the analysis of this study were processed and readapted multiple times, resulting in a basic IP setting that was found by consensus (M.S. and E.L.) to result in an overall good IQ.

The basic setting was subsequently modified to create five individual settings by varying the enhancement levels while keeping all other parameters constant: (A) high FE level, (B) high DRC enhancement level, (C) combination of A and B, (D) combination of A and B and high FNC enhancement level, and (E) combination of A and B and applied VGP (the exact parameter settings are shown in Supporting Information S2). Enhancement level differences were not maximized but adapted to a level still providing clinically adequate IQ in all five algorithm settings in 100% dose images. Gradation processing was not standardized as it could be individually adapted by each observer using the DICOM-viewer software.

2.2 Data recording and analysis

For image acquisition, a computed radiography storage system (FCR Profect CP Plus with HR-BD image plates, Fujifilm) was used (Table 1). Radiography of distal limbs was performed comparable with images in the upright pedal view (dorsal 80-degree proximal-palmarodistal and proximal-plantarodistal oblique views)²⁵ by placing the detector on the

table and positioning the limb directly on it. Physical antiscatter grids were not used.

The exposure settings were adjusted based on the manufacturer's recommendations for dose indicator values. For HR-BD image plates, the manufacturer recommends an aspired S-value in the range of 100. Exposure settings of 64.5 kVp and 8 mAs were estimated to reach the targeted S-value of 100 ± 10 (100% dose) in all phantoms. This exact exposure setting also matched the recommendations for radiography of the equine distal phalanx. Halving and quartering the mAs values resulted in the 50% dose and 25% dose groups, respectively (Table 1). The individual radiographs were then adapted multiple times according to each predefined IP setting, quintupling the number of images, which were subsequently stored in the PACS system (JiveX Enterprise PACS; VISUS Health IT).

Radiographs were reviewed by three ECVDI-certified veterinary radiologists (E.L., C.R., and C.S.) and one ECVDI final-year radiology resident (K.L.). The decisions were not based on consensus but on individual opinions. A training session was conducted on the application of the grading system. The images were randomized, and the metadata were removed. Thus, the observers were blinded to animal identification, processing, and dose settings. A medical-grade grayscale monitor (EIZO RadiForce MX242W; EIZO Corporation) and commercial DICOM-viewer software (JiveX Diagnostic 5.5.2; VISUS Health IT) were used. The observers were permitted to use postprocessing for zoom, contrast, and density adaptation. The observation time was not limited.



TABLE 1 Technical equipment and exposure settings.

TABLE 1 Technical equipment and exposure settings.							
Technical information							
Manufacturer	Fujifilm, Tokyo, Japan						
CR reader	Fuji CR PROFECT CS Image reader (Model: CR-IR 363)						
Detector type	Fuji CR image plate for dual-sided mammography reading (HR-BD)						
Detector size	$24\times30\text{cm}^2$						
Matrix	4728 × 5928						
Spatial resolution (pixel/mm)	20						
Spatial resolution (lp/mm)	<10						
Reading greyscale	12 bits						
Exposure settings							
Film-focal distance (FFD)	100 cm						
Grid	No						
X-ray system	Siemens Optitop 150/40/80HC - 100						
Focus size	$0.6 \times 0.6 \text{mm}^2$						
Field size	$18\times28\text{cm}^2$						
Exposure setting, 100% S-value, 100 ± 10	64.5 kVp; 8 mAs						
Exposure setting, 50% S-value, 200 ± 20	64.5 kVp; 4 mAs						
Exposure setting, 25% S-value, 400 ± 40	64.5 kVp; 2 mAs						

Abbreviation: CR, computed radiography.

Seven image criteria, comprising five anatomical structures (A—trabecular bone, B—navicular bone, C—vascular channels, D—extraarticular soft-tissue structures, and E—frog) and two technical features (F—image noise and G—Überschwinger artifact), were evaluated using a five-point scoring system ranging from 1 (best) to 5 (worst). Table 2 presents a detailed description of the assessment of each criterion. The anatomical structures are shown in Figure 2. The two technical features were assessed in selected areas, as shown in Figure 2. Each criterion was scored individually, but for further analyses, criteria A–C were subsumed as bone structures and criteria D and E were subsumed as soft-tissue structures. The images were rated without reference images.^{26,27}

2.3 | Statistics

Statistical tests were selected by an ECVDI-certified veterinary radiologist (E.L.) with statistical experience in performing similar studies, and the analysis was carried out by a graduate student (M.S.) with training in biostatistics as part of his doctoral degree (DrVetMed). Scoring frequencies, mean values, and 95% confidence intervals were calculated to facilitate comparisons between IP settings and review-

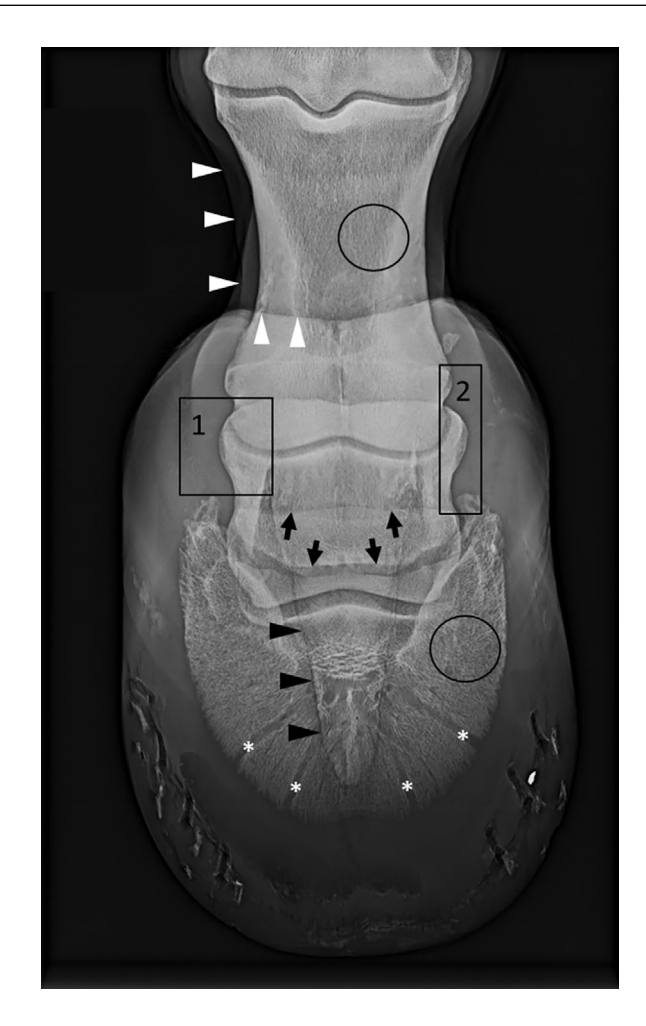


FIGURE 2 Dorsal 80-degree proximal-palmarodistal oblique (D80Pr-PaDiO) radiograph of an equine distal forelimb. The criteria listed in Table 2 are marked: A, trabecular bone (black circle); B, navicular bone (black arrows); C, vascular channels (asterisks); D, extraarticular soft tissues (white arrowheads); E, frog (black arrowheads); F, image noise (box 1); G, Überschwinger artifact (box 2).

ers (Microsoft Excel 2019, Microsoft Corporation). To calculate the intersystem IQ variability, absolute visual grading characteristic (VGC) analyses were performed as described elsewhere.²⁷ The outcome reflects the observer's confidence in assessing the predefined criteria without using reference images. Because of the methodical parallels of this method with receiver operating characteristic analyses, ²⁷ ROC software (IBM SPSS Statistics 26, IBM) was used to generate graphs and to estimate areas under the curves (AUCs), confidence intervals, and P-values. The more the AUC deviated from 0.5, the more the two IP settings systems differed in their IQ. Statistical significance was set at P < .05. Spearman's rank correlation was applied to evaluate interobserver correlation (IBM SPSS Statistics 26). Correlations were considered significant at P < .05. The effect size of correlation was "negligible" for r < 0.1, "low" for r between 0.1 and 0.3, "moderate" for r between 0.3 and 0.5, and "high" for r > 0.5.²⁸ In addition, interobserver agreement was calculated using Cohen's kappa test with the same significance levels and effect sizes as described above.

TABLE 2 Assessment criteria and scoring system used by observers for evaluating image quality.

Criteria—anatomical structures		Definition			
A	Trabecular bone ^a	Discrimination between compact and trabecular bone, identification of the trabecular bone structure in the nonsuperimposed part of the proximal and distal phalanx			
В	Navicular bone ^a	Contrast and delineation of the bony contour of the navicular bone			
С	Vascular channels ^a	Demarcation of vascular channels from the sole canal to the sole border of the distal phalanx			
D	Extraarticular soft-tissue structures ^b	Delineation of the caudal border of the bulb and the boundary of soft tissues			
E	Frog ^b	Demarcation of the frog			
Criteria—technical features		Definition			
F	Image noise	Image noise level; influence on the depiction of anatomical structures			
G	Überschwinger artifact	Rebound artifact level; influence on the depiction of anatomical structures			
Scoring system for A-E		Definition			
1	Excellent	Structures are completely evaluable, textbook-quality			
2	Good	Structures are evaluable, no limitations for clinical interpretation			
3	Sufficient	$Structure\ evaluation\ is\ possible, minor\ limitations\ for\ clinical\ interpretation$			
4	Limited	Structure evaluation is restricted, major limitations for clinical interpretatio			
5	Insufficient	No interpretation possible			
Scoring system for F and G		Definition			
1	Excellent	No loss of information			
2	Good	Minor loss of information, no restriction on structure assessment			
3	Sufficient	Minor loss of information, minor restriction on structure assessment			
4	Limited	Major loss of information, structure assessment limited			
5	Insufficient	Major loss of information, structure assessment not possible			

^aCriteria A-C were subsumed as bone structures.

3 | RESULTS

The analysis was based on a total of 8400 individual observer decisions.

3.1 | Overall algorithm comparisons

For all reviewers combined, 43.3% (13/30) significant differences between algorithms based on AUC $_{VGC}$ comparisons were found (Supporting Information S3). At 100% dose, IP algorithms were overall ranked as follows (from best to worst): D–E–B–A–C (mean scores, 1.75–1.86). However, at lower doses, the ranking changed (Figure 3; ranking shown in Table 3; and numerical data shown in Supporting Information S5).

The suitability of the algorithms for a clinical setting was evaluated by assessing the percentage of limited and insufficient ratings (i.e., scores of 4 and 5). This was <4% of ratings for all algorithms at 100% dose; 4%-10% of ratings at 50% dose (the lowest rating for algorithm D with 4.2% of ratings); 18.8% (D) to 43.6% (C) at 25% dose (Figure 4, Supporting Information S6).

3.2 | Algorithm comparisons according to individual image criteria

A detailed overview of the criteria scores for the individual doses and algorithms is shown in Figure 5 and Supporting Information S6. The AUC $_{\rm VGC}$ values of the algorithm comparisons and significance levels are shown in Supporting Information S3. The rankings of the algorithms are listed in Table 3. The most important observations are summarized below. The percentages of limited and insufficient ratings (i.e., scores of 4 and 5) for the individual image criteria are shown in Figure 4 and Supporting Information S6. Figure 6 is an example of algorithm performance on an identical radiograph, comparing 100% and 25% doses.

3.2.1 | Bone structures

The perception of bone structures was better with VGP (algorithm E) than without it (algorithm C) at all three dose levels. Differences were not observed with FNC enhancement (algorithm D) and without

^bCriteria D and E were subsumed as soft-tissue structures.

, Wiley Online Library on [02/07/2025]. See

TABLE 3 Performance of algorithms A-E ranking from best (left) to worst (right).

Criteria	Dose level (%)	Algorithm ranking (best to worst)					
Bone structures	100	ECBA	D^BA	C ^A	В	Α	
	50	E _{BAC}	D^BAC	B↑	A↑	C↓	
	25	$D^{BEAC} \!\!\uparrow$	$B^AC\!\!\uparrow$	$E^{AC}\!\downarrow$	$A^C\!\!\uparrow$	C↓	
Soft-tissue structures	100	E	D	С	В	Α	
	50	D↑	E↓	B↑	A↑	C↓	
	25	D ^c ↑	B ^C ↑	A ^c ↑	E↓	C↓	
Image noise	100	B_{EC}	DEC	A^{EC}	Е	С	
	50	B ^{AEC}	DEC	A^c	Ec	С	
	25	B ^{AEC}	D ^{AEC}	A^c	Ec	С	
Überschwinger artifact	100	A ^{BCDE}	B^E	C_E	D^E	Е	
	50	ABCDE	B^E	C_E	D^E	Е	
	25	A ^{CDE}	B^E	C_E	D^E	E	
All criteria	100	Dc	Е	В	Α	С	
	50	D_C	$B^C\!\uparrow$	A ^c ↑	$E_C \!\!\downarrow$	С	
	25	D ^{ACE}	$B^{ACE}\!\!\uparrow$	A ^c ↑	$E_C \!\!\downarrow$	С	

Note: Superscript letters indicate algorithms that are significantly worse in AUC_{VGC} analyses. Algorithms ranked better and worse in lower-dose images in comparison with the 100%-dose ranking are marked with an arrow pointing up and down, respectively.

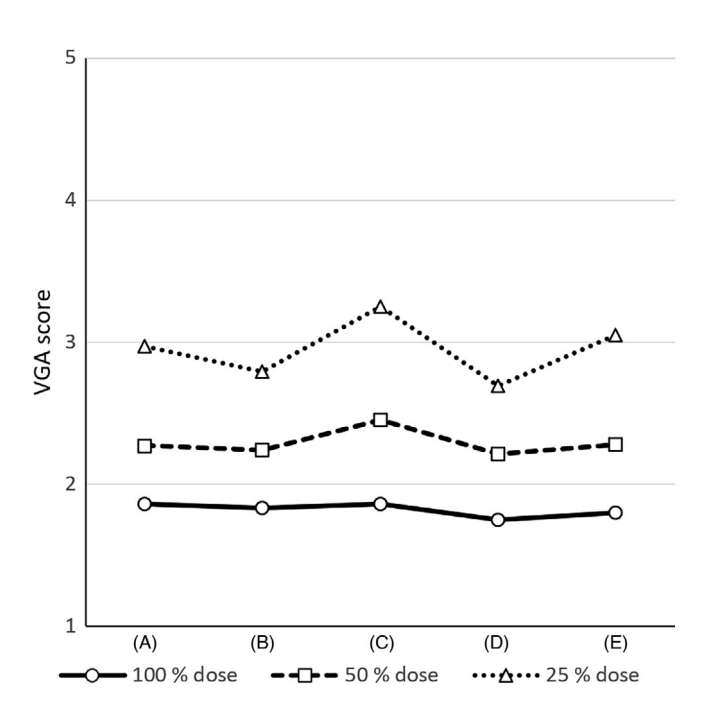


FIGURE 3 Mean scores of individual algorithms including all criteria and all reviewers at 100%, 50%, and 25% doses. The five-point scoring system ranges from 1 (best) to 5 (worst). Numeric values are shown in Supporting Information S5.

FNC enhancement (algorithm C) at 100% dose, but bone structure perception was better with FNC enhancement at lower dose levels. Finally, bone structure perception was better with both FE and DRC enhancement (algorithm C) than with only FE (algorithm A) at 100% dose.

3.2.2 | Soft-tissue structures

Mean scores were significantly different only at 25% dose.

3.2.3 Image noise

At all three dose levels, image noise perception was lower with FNC enhancement (algorithm D) than without FNC enhancement (algorithm C), and lower with only DRC enhancement (algorithm B) than with FE and DRC enhancement (algorithm C). At 50% dose, scores were not lower than sufficient for algorithms B and D (Figure 4, Supporting Information S6).

Überschwinger artifact 3.2.4

At all three dose levels, Überschwinger artifact perception was higher with VGP (algorithm E) than without VGP (algorithm C) and lower without DRC enhancement (algorithm A) than with DRC enhancement (algorithm C).

3.3 Dose effects

The criterion that was most affected by the image dose was image noise. The criterion least affected was the Überschwinger artifact (Supporting Information S6). To evaluate the potential of dose reduction by changing the algorithm, we compared 100%-dose image scores of each

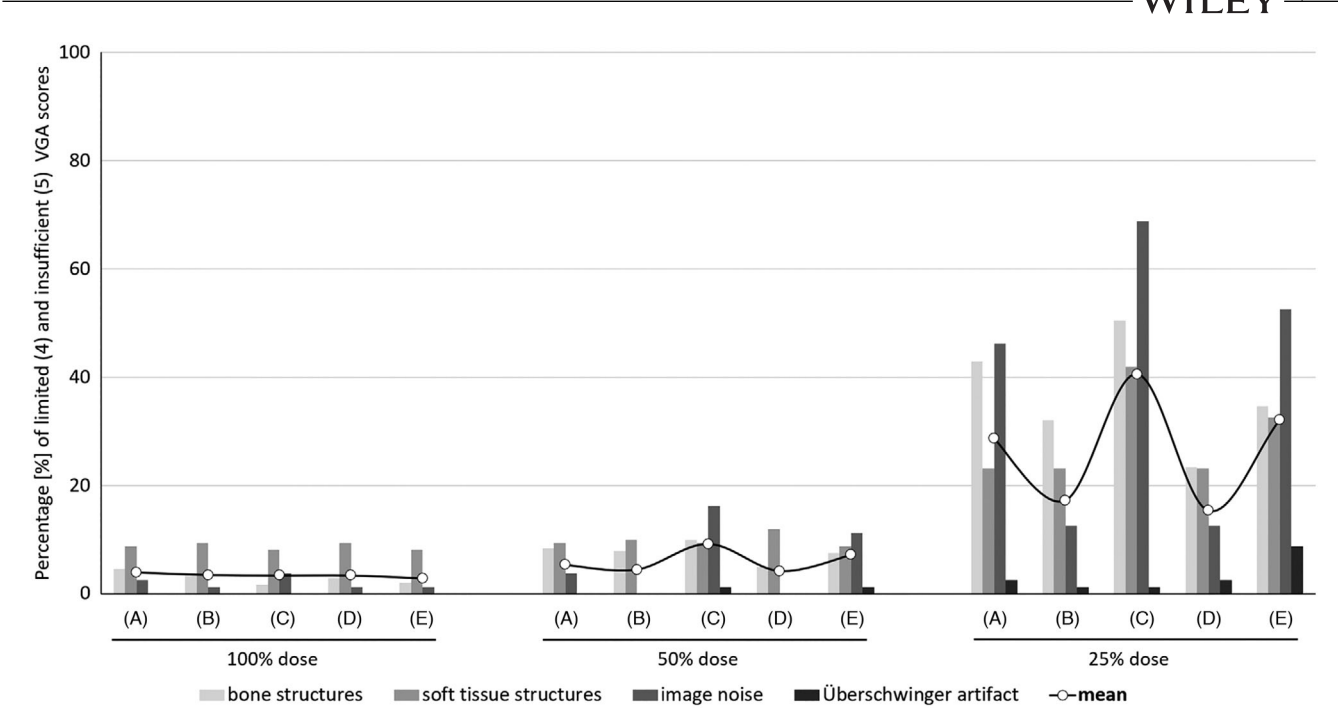


FIGURE 4 Percentage of images that were rated lower than "sufficient" (i.e., "limited" [score 4] and "insufficient" [score 5]) at 100%, 50%, and 25% doses for individual criteria: bone structures, soft-tissue structures, image noise, and Überschwinger artifact. Mean values are indicated with white circles. Numeric values are shown in Supporting Information S3 and S5.

criterion with lower-dose (50% and 25%) image scores of the same criterion processed with a different algorithm. By changing the algorithm, the criteria bone structures and soft-tissue structures were still rated significantly worse in AUC_{VGC} analysis in all cases for images with a reduced dose (Supporting Information S6). However, a change to an alternative algorithm resulted in a better IQ in lower-dose images (e.g., changing algorithm C to D), as described above.

3.4 Interobserver comparisons

At the 100%-dose level, individual reviewers differed regarding their best- and worst-rated IP algorithm. With decreasing doses, the assessments were more uniform among observers: algorithm C was ranked worst by 4 of 4 reviewers, and algorithm D was ranked best by 3 of 4 reviewers (Supporting Information S5).

Interobserver correlations and agreements were calculated for all observers and all imaging criteria. Interobserver correlation was significant in 92.9% (39/42) of the cases. The Spearman correlation coefficients ranged from 0.023 to 0.727 with a mean value of 0.375, indicating an overall moderate correlation. The correlation was lowest for extraarticular soft-tissue structures (mean value of 0.167) and highest for image noise (mean value of 0.615). The interobserver agreement was significant in 69.0% (29/42) of the cases. Image noise was the only criterion for which all correlations were significant. Cohen's kappa coefficients ranged from 0.011 to 0.391, with a mean value of 0.121, indicating an overall low agreement. The agreement was lowest

for frog (mean value of 0.051) and highest for image noise (mean value of 0.242).

4 | DISCUSSION

This experimental study investigated the influence of IP on IQ in the computed radiography of equine distal limbs. The findings of this study supported our first hypothesis, as different IP settings influenced the perception of predefined image criteria, and this influence was greater for bone structures and at low detector doses. The second hypothesis was partially accepted, as VGP enhanced the perception of bone structures, but no effect could be shown on the perception of softtissue structures. The third hypothesis was accepted as the perception of anatomic criteria improved at low levels of detector doses with FNC enhancement. The fourth hypothesis was partially accepted, as the ranking of IP settings was different at full and low levels of detector dose for anatomic criteria but not for technical features. A clinically acceptable IQ could be maintained at a 50% dose with the FNC enhancement setting but not at a 25% dose. The fifth hypothesis was partially accepted because the preference for individual algorithms at the full dose varied among observers. However, agreement was high at low-detector doses. The results of the present study are consistent with previous findings in human orthopedic radiography 15,29,30 and expand the proven applicability of IP to equine radiography. Based on our literature review, this is the first study to focus on IQ optimization using IP, including MFP, FNC, and VGP in equine radiography.

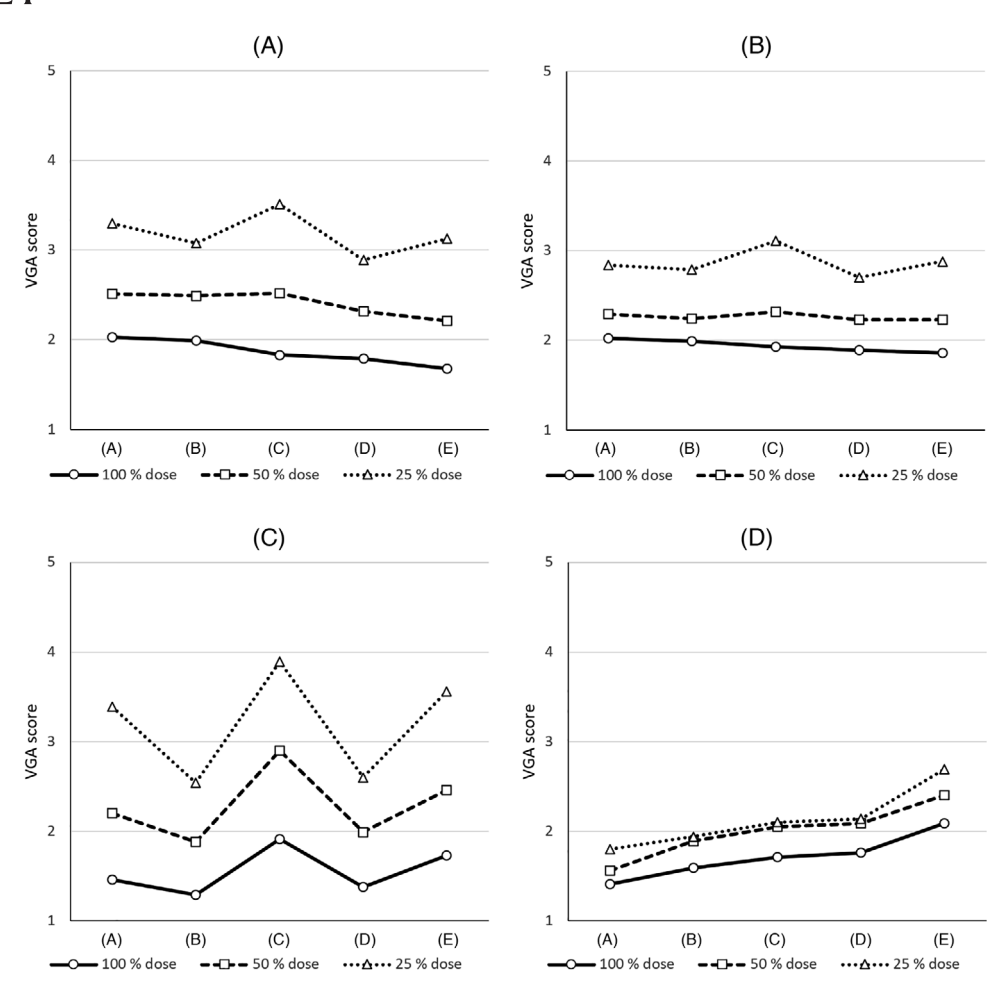


FIGURE 5 Mean algorithm scores for individual criteria: A, bone structures; B, soft-tissue structures; C, image noise; and D, Überschwinger artifact at 100%, 50%, and 25% doses. The five-point scoring system ranges from 1 (best) to 5 (worst). Numeric values are shown in Supporting Information S6.

IQ in digital radiography is not easy to define, as it depends on the clinical question and the observer's preference. One measure of IQ is the visibility of anatomical structures, as used in VGA, which has been shown to be strongly correlated with the detectability of pathological structures. In our study, five anatomical criteria were established. Unlike human medicine, were chosen to cover the relevant parameters for radiographic IQ 26 : spatial resolution (trabecular bone), low-contrast resolution (extraarticular soft-tissue structures, frog), and high-contrast resolution in both small (vascular channels) and large (navicular bone) structures. Additionally, two criteria were chosen to evaluate the impact of processing artifacts on IQ (image noise, Überschwinger artifact). In

Overall, individual IP settings influence IQ but to varying degrees in different structures. At the predefined 100% dose, the perception of soft-tissue structures was not significantly affected by any chosen algorithm. Conversely, the perception of bone structures was deemed the best with VGP. Scatter radiation compromises IQ by creating unwanted generalized exposure called "fog" which reduces contrast and adds quantum noise. 13 Manufacturers have released scatter correction soft-

ware as an alternative to physical grids. 18 Unlike a physical grid, scatter radiation is not filtered out prior to absorption by the detector; rather, mathematical algorithms calculate the components of the expected scatter radiation in the signal. 18 As a result, subjective contrast was restored, as demonstrated by thoracic radiography in humans^{7,19} and animals. 10 A recent study reported the same beneficial effect on bone structure perception in human skeletal radiography, 30 which is consistent with our results. Disruptive scatter radiation occurs when object diameters are greater than 10 cm¹³; thus, low amounts of scatter radiation are expected. However, previous studies have found that scatter correction software also shows a positive effect in anatomic regions where low amounts of scatter radiation are expected. 30,19 Physical antiscatter grids are not routinely used in the radiography of equine distal limbs, as they entail a substantial increase in exposure dose, and positioning is time-consuming. Our results suggest that VGP has the potential to improve the perception of bone structures. However, further studies comparing VGP and physical antiscatter grid images, as performed in human radiography,⁷ are needed.

We demonstrated that a combination of high enhancement levels of FE and DRC leads to a good perception of bone structures in 100% dose

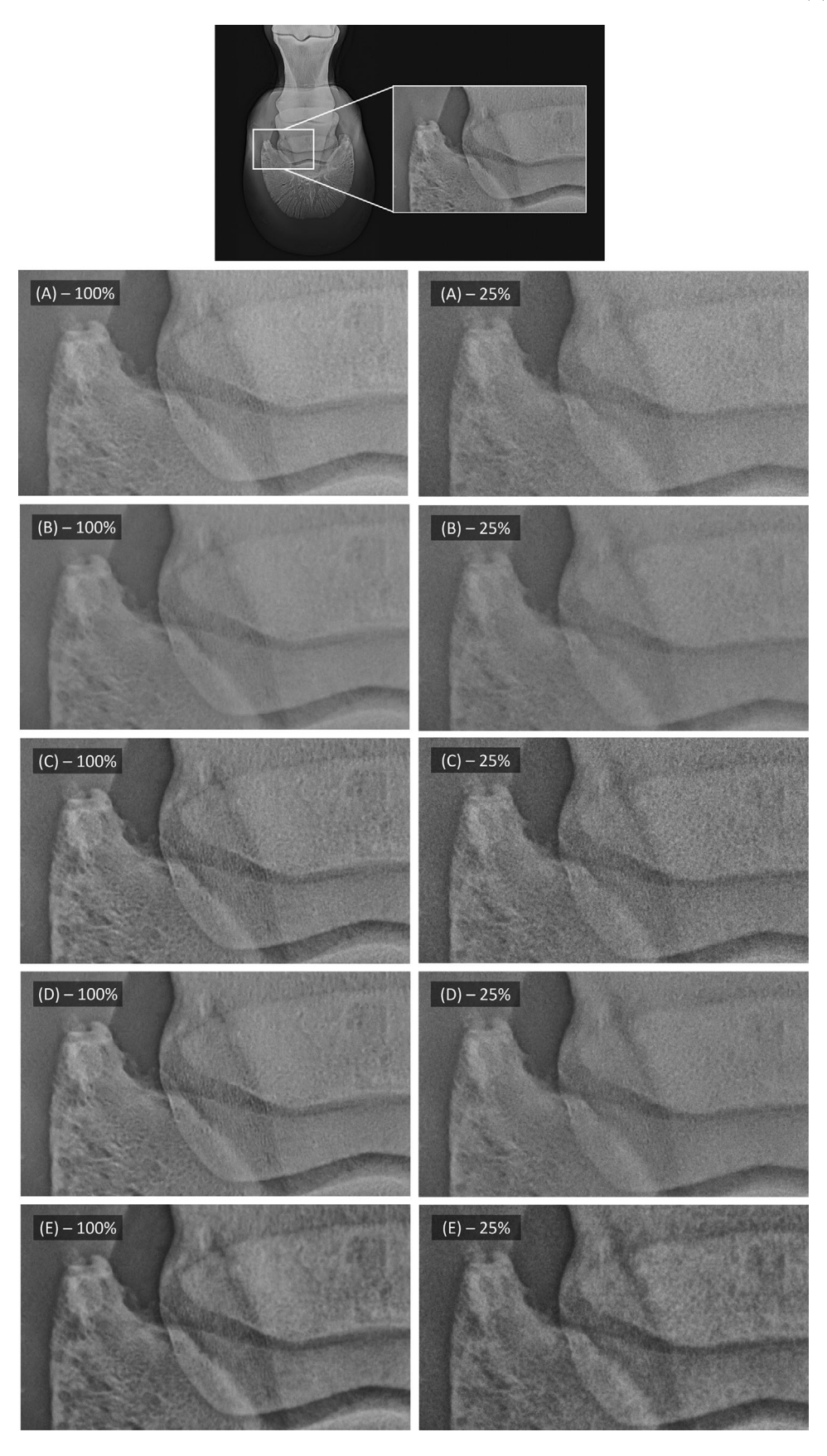


FIGURE 6 The images represent examples of the different image processing algorithms acquired at 100% and 25% doses from the same distal limb.

images. Our results are consistent with those of other studies showing that MFP can increase IQ in human skeletal radiography. This can be explained by the two complementary functions of the MFP to improve contrast: hard-to-detect (low-contrast) structures are enhanced by FE, and conventional over- or underexposed regions are better displayed by DRC. A,5,33 A description of the mathematical background of the MFP5 is beyond the scope of this study; however, it is comparable to the multiscale filters of other providers. A Caution should be taken, as overenhancement has been shown to suppress normal bone density and simulate osteoporosis.

Überschwinger artifact (overshoot or rebound effect) appears as a radiolucent halo around areas with large density differences between adjacent objects. ¹⁷ This artifact had little influence on IQ in our study setting, as the worst score was between "sufficient" and "good". In contrast to older unsharp-mask processing, MFP⁵ and especially the second-generation system Dynamic Visualization II³³ can minimize this artifact. Nonetheless, we did find differences between algorithms: VGP led to a higher level of Überschwinger artifact recognition than other IP settings. Reducing the DRC enhancement level was the best way to address this problem. Überschwinger artifacts can simulate the loosening of orthopedic devices or mimic pneumothorax. ¹⁷ Thus, in clinical settings, when it is questionable whether an actual pathology or an artifact is present, images can be reprocessed without VGP and with a low DRC.

In this study, the perception of anatomical structures in low-dose images could not be fully compensated for by adjusting the IP settings. Other studies found that a dose reduction of up to 61% was possible using IP software. 7,8 However, these studies only compared softwareprocessed and nonprocessed images. Although the overall perception of anatomical structures was slightly worse, in clinical practice, a dose reduction of 50% appears acceptable with IP adaptation. In lowdose images, the enhanced-contrast algorithms that performed well in adequately dosed images (algorithms A and C) were outperformed by the noise-suppressing algorithms (algorithms B and D) regarding bone structure perception. Thus, in accordance with the ALARA guidelines,³⁵ if a radiograph is underexposed, it could be assessed whether an IP adaptation can improve the IQ sufficiently to answer the clinical question before the image is repeated at a higher dose. Another advantage is that underexposed images that are reviewed after the animal has already left can be improved without the need for a recall.

Image noise was the factor most affected by dose reduction. Noise itself originates from various sources with quantum noise being the most dominant source in low-dose images.³⁶ A common method for reducing the effects of quantum noise is to increase the detector exposure. Software-based virtual noise reduction yields very similar results.³⁷ In our study it was possible to reduce the detector dose to 50% maintaining an acceptable level of image noise perception. The first option is to lower the FE level, and the second option relies on increasing the FNC enhancement level. When image contrast is enhanced via FE changes, noise is also emphasized.^{17,33} Thus, if high quantum noise is present, as in low-dose imaging, enhancing the contrast with FE leads to an accentuation of the already present noise, and the FE process thus may be deleterious.⁵ The second option is prefer-

able as it allows us to maintain a higher FE level and to better assess bone structures. ²¹ In agreement with our results, previous studies have shown that FNC is an effective approach to reduce noise in human radiography. ^{4,15} FNC is a multiresolution filter, which in contrast to a simple average filter (i.e., linear low-pass filters) does not blur the whole image but is able to preserve edges and anatomical structures. ⁴

The overall correlation among the observers was moderate and comparable to that of other observational studies with similar study designs. Although the reviewers were not necessarily expected to provide the same scores, it was interesting to determine if the trends were similar. The low correlations in the evaluation of anatomical structures can be adequately explained by the fact that the observers had different algorithm preferences at full dose, possibly because all algorithms performed well at this dose. In contrast, the correlation was high for image noise perception. At reduced doses, the differences in IQ among algorithms were greater, and all observers agreed that noise suppression algorithms (algorithms B and D) should be preferred. As all observers were experienced in radiology, the criteria were simple to evaluate, and the evaluation scheme was explained in training sessions, the differences in algorithm preference could be best explained by personal taste. 15,31

Our study has several limitations. There are no standard or recommended IP settings for equine distal limbs. The algorithms used were chosen subjectively and can only be compared with each other. By selecting a higher difference in IP parameters between algorithms, a greater difference in IQ can be suspected. Thus, in cases in which we found no significant differences, it cannot be claimed that IP has, in general, no influence on specific criteria. The different algorithms are based on differences in the enhancement level, while other parameters were kept constant (e.g., balance type and enhancement type) so that their influence on IQ could not be assessed. An investigation of all parameters is beyond the scope of this study. Absolute VGC analysis is based on a subjective assessment of IQ; therefore, the results depend on the observer's opinion.³⁸ However, this method was described as appropriate for evaluating IQ in diagnostic imaging^{26,27} and previously used in comparable studies, 8,19,20,30,34 reflecting everyday clinical practice. Furthermore, a possible confounding effect of phantom variability was considered in the study design, as it had an equally weighted influence on all IP algorithms and dose levels. However, equine distal limbs, like any other region of the body, come in different conformations and sizes. The possible influence of the phantom size should be investigated in further studies. We tested the influence of IP on IQ using Fuji software. Each provider developed its own IP software.³⁴ Although the underlying technical principles overlap,⁵ our results cannot be fully transferred to the software of other providers.

In conclusion, IP settings had a significant influence on the radiologists' perception of IQ, and this influence was greater at low detector doses. The perception of predefined bone structures was best at full detector doses with VGP and at low detector doses with FNC enhancement. The ranking of the investigated IP settings differed according to predefined anatomical and technical criteria, detector doses, and reviewers. Thus, the findings supported using individualized IP settings

based on the radiologist's preferences and situational image requirements, rather than using default settings. Further studies are needed to test the influence of other IP parameters on IQ, as well as in smaller animals and in other anatomical regions that may have different IP requirements.

ACKNOWLEDGEMENTS

The authors acknowledge the Institute of Pathology, University of Veterinary Medicine, Vienna, for providing and preparing the distal limbs of equine cadavers. The authors also acknowledge FUJIFILM Healthcare, Austria for contributing content related to the image processing software.

LIST OF AUTHOR CONTRIBUTIONS

Category 1

- a. Conception and design: Ludewig, Seeber, Rowan, Lederer, Strohmayer
- b. Acquisition of data: Seeber
- c. Analysis and interpretation of data: Seeber

Category 2

- a. Drafting the article: Seeber, Ludewig, Rowan
- b. Revising article for intellectual content: Ludewig, Seeber, Rowan, Lederer, Strohmayer

Category 3

a. Final approval of the completed article: Ludewig, Seeber, Rowan, Lederer, Strohmayer

Category 4

a. Agreement to be accountable for all aspects of the work in ensuring that questions related to the accuracy or integrity of any part of the work are appropriately investigated and resolved: Ludewig, Seeber, Rowan, Lederer, Strohmayer

CONFLICT OF INTEREST STATEMENT

The authors declare no conflict of interest.

PREVIOUS PRESENTATION DISCLOSURE

The findings of the present study have neither been reported in a previous meeting nor published in an abstract.

REPORTING GUIDELINE DISCLOSURE

The STROBE checklist was used in the preparation of this manuscript.

DATA AVAILABILITY STATEMENT

Data supporting the findings of this study are available as supplementary files and from the corresponding author upon reasonable request.

ORCID

Matthias Seeber https://orcid.org/0009-0004-7565-1710 Carina Strohmayer https://orcid.org/0000-0002-6552-357X

REFERENCES

- 1. Dixon J, Biggi M, Weller R. Common artefacts and pitfalls in equine computed and digital radiography and how to avoid them. Equine Vet Educ. 2018;30:326-335. doi:10.1111/eve.12595
- 2. Båth M, Håkansson M, Hansson J, Månsson LG. A conceptual optimisation strategy for radiography in a digital environment. Radiat Prot Dosim. 2005;114:230-235. doi:10.1093/rpd/nch567
- 3. Lo WY, Puchalski SM. Digital image processing. Vet Radiol Ultrasound. 2008; 49:S42-S47. doi:10.1111/j.1740-8261.2007.00333.x
- 4. Yamada S, Murase K. Effectiveness of flexible noise control image processing for digital portal images using computed radiography. Br J Radiol. 2005;78:519-527. doi:10.1259/bjr/26039330
- 5. Prokop M. Neitzel U. Schaefer-Prokop C. Principles of image processing in digital chest radiography. J Thorac Imaging. 2003;18:148-164. doi:10.1097/00005382-200307000-00004
- 6. Don S, Whiting BR, Ellinwood JS, Foos DH, Kronemer KA, Kraus RA. Neonatal chest computed radiography: image processing and optimal image display. AJR Am J Roentgenol. 2007;188:1138-1144. doi:10. 2214/AJR.05.0733
- 7. Ahn SY, Chae KJ, Goo JM. The potential role of grid-like software in bedside chest radiography in improving image quality and dose reduction: an observer preference study. Korean J Radiol. 2018; 19:526-533. doi:10.3348/kjr.2018.19.3.526
- 8. Precht H, Gerke O, Rosendahl K, Tingberg A, Waaler D. Digital radiography: optimization of image quality and dose using multi-frequency software. Pediatr Radiol. 2012;42:1112-1118. doi:10.1007/s00247-012-2385-3
- 9. Lo WY, Hornof WJ, Zwingenberger AL, Robertson ID. Multiscale image processing and antiscatter grids in digital radiography. Vet Radiol Ultrasound. 2009;50:569-576. doi:10.1111/j.1740-8261.2009.01585.
- 10. Shimbo G, Tagawa M, Matsumoto K, Tomihari M, Miyahara K. Effects of scatter correction processing on image quality of portable thoracic radiography in calves. Jpn J Vet Res. 2018; 66:105-112. doi:10.14943/ jjvr.66.2.105
- 11. Kleinfelder TR, Curtis CK. Effects of Image postprocessing in digital radiography to detect wooden, soft tissue foreign bodies. Radiol Technol. 2022:93:544-554.
- 12. Whitlock J, Dixon J, Sherlock C, Tucker R, Bolt DM, Weller R. Technical innovation changes standard radiographic protocols in veterinary medicine: is it necessary to obtain two dorsoproximal-palmarodistal oblique views of the equine foot when using computerised radiography systems? Vet Rec. 2016;178:531. doi:10.1136/vr.103396
- 13. Thrall DE, Widmer WR. Textbook of Veterinary Diagnostic Radiology. 7th ed. Elsevier: 2018:986.
- 14. Uffmann M, Schaefer-Prokop C. Digital radiography: the balance between image quality and required radiation dose. Eur J Radiol. 2009;72:202-208. doi:10.1016/j.ejrad.2009.05.060
- 15. Precht H, Waaler D, Outzen CB, et al. Does software optimization influence the radiologists' perception in low dose paediatric pelvic examinations? Radiography. 2019; 25:143-147. doi:10.1016/j. radi.2018.12.013
- 16. Lisson CG, Lisson CS, Kleiner S, Regier M, Beer M, Schmidt SA. Iterative scatter correction for grid-less skeletal radiography allows improved image quality equal to an antiscatter grid in adjunct with dose reduction: a visual grading study of 20 body donors. Acta Radiol. 2019;60:735-741. doi:10.1177/0284185118796668
- 17. Drost WT, Reese DJ, Hornof WJ. Digital radiography artifacts. Vet Radiol Ultrasound. 2008;49:S48-56. doi:10.1111/j.1740-8261.2007. 00334.x

- Kawamura T, Naito S, Okano K, Yamada M. Improvement in image quality and workflow of X-ray examinations using a new image processing method, "Virtual Grid technology". Fujifilm Res Dev. 2015;60:21-27.
- Renger B, Brieskorn C, Toth V, et al. Evaluation of dose reduction potentials of a novel scatter correction software for bedside chest X-ray imaging. *Radiat Prot Dosim.* 2016;169:60-67. doi:10.1093/rpd/ ncw031
- Tebrün W, Ludewig E, Köhler C, Böhme J, Pees M. Needle-based storage-phosphor detector radiography is superior to a conventional powder-based storage phosphor detector and a high-resolution screen-film system in small patients (budgerigars and mice). Sci Rep. 2019;9:10057. doi:10.1038/s41598-019-46546-5
- 21. Jadidi M, Båth M, Nyrén S. Dependency of image quality on acquisition protocol and image processing in chest tomosynthesis-a visual grading study based on clinical data. *Br J Radiol.* 2018;91:20170683. doi:10.1259/bjr.20170683
- 22. Notohamiprodjo S, Roeper KM, Mueck FG, et al. Advances in multiscale image processing and its effects on image quality in skeletal radiography. *Sci Rep.* 2022;12:4726. doi:10.1038/s41598-022-08699-8
- Bochmann M, Ludewig E, Krautwald-Junghanns ME, Pees M. Comparison of the image quality of a high-resolution screen-film system and a digital flat panel detector system in avian radiography. Vet Radiol Ultrasound. 2011;52:256-261. doi:10.1111/j.1740-8261.2011.01801.
- 24. Moore CS, Liney GP, Beavis AW, Saunderson JR. A method to optimize the processing algorithm of a computed radiography system for chest radiography. *Br J Radiol*. 2007;80:724-730. doi:10.1259/bjr/33261679
- Díaz GM, López-Sanromán J, Weller R. A Practical Guide to Equine Radiography. 5M Publishing Ltd. Sheffield, UK. 2018:222.
- Precht H, Hansson J, Outzen C, Hogg P, Tingberg A. Radiographers' perspectives' on visual grading analysis as a scientific method to evaluate image quality. *Radiography*. 2019;25:14-S18. doi:10.1016/j.radi. 2019.06.006
- Båth M, Månsson LG. Visual grading characteristics (VGC) analysis: a non-parametric rank-invariant statistical method for image quality evaluation. Br J Radiol. 2007;80:169-176. doi:10.1259/bjr/35012658
- Cohen J. A power primer. Psychol Bull. 1992;112:155-159. doi:10. 1037//0033-2909.112.1.155
- Sasagawa T, Kunogi J, Masuyama S, et al. New computed radiography processing condition for whole-spine radiography. *Orthopedics*. 2011;34:906-910. doi:10.3928/01477447-20111021-15
- Lisson CG, Lisson CS, Vogele D, et al. Improvement of image quality applying iterative scatter correction for grid-less skeletal radiography in trauma room setting. Acta Radiol. 2020;61:768-775. doi:10.1177/ 0284185119878348

- Decoster R, Mol H, Smits D. Post-processing, is it a burden or a blessing? Part 1 evaluation of clinical image quality. *Radiography*. 2015;21:e1-e4. doi:10.1016/j.radi.2014.06.003
- Sund P, Båth M, Kheddache S, Månsson LG. Comparison of visual grading analysis and determination of detective quantum efficiency for evaluating system performance in digital chest radiography. Eur Radiol. 2004;14:48-58. doi:10.1007/s00330-003-1971-z
- Takahashi T, Ohara Y, Yamada M. Improving X-ray image quality based on human-body thickness and structure recognition. Fujifilm Res Dev. 2017;62:30-37.
- Smet MH, Breysem L, Mussen E, Bosmans H, Marshall NW, Cockmartin L. Visual grading analysis of digital neonatal chest phantom X-ray images: impact of detector type, dose and image processing on image quality. Eur Radiol. 2018;28:2951-2959. doi:10.1007/s00330-017-5301-2
- Willis CE, Slovis TL. The ALARA concept in pediatric CR and DR: dose reduction in pediatric radiographic exams—a white paper conference.
 AJR Am J Roentgenol. 2005;184:373-374. doi:10.1007/s00247-004-1264-y
- Cerciello T, Bifulco P, Cesarelli M, et al. Noise reduction in fluoroscopic image sequences for joint kinematics analysis. Paper presented at: XII Mediterranean Conference on Medical and Biological Engineering and Computing: MEDICON 2010, May 27–30, 2010, Chalkidiki, Greece.
- Bernhardt P, Lendl M, Deinzer F. New technologies to reduce pediatric radiation doses. *Pediatr Radiol.* 2006;36:212-215. doi:10.1007/s00247-006-0212-4
- Keeble C, Baxter PD, Gislason-Lee AJ, Treadgold LA, Davies AG. Methods for the analysis of ordinal response data in medical image quality assessment. Br J Radiol. 2016;89:20160094. doi:10.1259/bjr. 20160094

SUPPORTING INFORMATION

Additional supporting information can be found online in the Supporting Information section at the end of this article.

How to cite this article: Seeber M, Lederer KA, Rowan C, Strohmayer C, Ludewig E. Image processing setting adaptions according to image dose and radiologist preference can improve image quality in computed radiography of the equine distal limb: A cadaveric study. *Vet Radiol Ultrasound*. 2024;65:19–30. https://doi.org/10.1111/vru.13321